Variational Image Segmentation Using Boundary Functions

Gary A. Hewer, Charles Kenney, and B. S. Manjunath, *Member, IEEE*

***Abstract*—A general variational framework for image approximation and segmentation is introduced. By using a continuous "line-process" to represent edge boundaries, it is possible to formulate a variational theory of image segmentation and approximation in which the boundary function has a simple explicit form in terms of the approximation function. At the same time, this variational framework is general enough to include the most commonly used objective functions. Application is made to Mumford–Shah type functionals as well as those considered by Geman and others. Employing arbitrary L_p norms to measure smoothness and approximation allows the user to alternate between a least squares approach and one based on total variation, depending on the needs of a particular image. Since the optimal boundary function that minimizes the associated objective functional for a given approximation function can be found explicitly, the objective functional can be expressed in a reduced form that depends only on the approximating function. From this a partial differential equation (PDE) descent method, aimed at minimizing the objective functional, is derived. The method is fast and produces excellent results as illustrated by a number of real and synthetic image problems.**

***Index Terms*—Boundary functions, variational segmentation.**

I. Introduction

In THIS paper, a general variational framework is presented for image segmentation and approximation. In addition to several new results, one of the main contributions is in simplifying and systematizing approaches that had previously been considered separately, especially those with Mumford–Shah objective functionals [13]–[15] and those considered by Geman and others [6]–[8]. The common framework for these approaches also makes it much easier to do comparative studies of competing systems.

To set the stage, suppose that we are given a blurred image g over a domain Ω:

$$g = Au_0 + \eta \tag{1}$$

where A is the blurring operator, u_0 is the unblurred image, and η is the noise. One approach to segmenting and approximating such an image consists of finding an approximation u and a boundary set K that minimizes an objective functional of the form

$$\tilde{E}(u, K) = w_1 \int_{\Omega\backslash K} (Au - g)^2 + w_2 \int_{\Omega\backslash K} \nabla u \cdot \nabla u + w_3 \int_K d\sigma \tag{2}$$

where the last integral term corresponds to the length of the boundary. The scalars w_1, w_2, and w_3 are weighting factors that determine, respectively, how closely Au approximates g, the smoothness of u and the extent of the boundary. Without loss of generality we may assume that $w_3 = 1$. Functionals of this type are often referred to as *Mumford–Shah functionals*. See [12, p. 24]–[15] for details.

Unfortunately numerical procedures for minimizing the Mumford–Shah functional encounter bookkeeping problems associated with tracking regions and their boundaries. These problems can be traced to the binary nature of the boundary description as embodied in the boundary characteristic function χ, which takes on the value 1 on the boundary K and zero elsewhere. Binary descriptions of boundaries may be appropriate in some special cases but for most problems the transitions between regions can occur over several pixels rather than abruptly. Moreover the mathematical view of the boundary as the differential of a region (hence the notation ∂R for the boundary of a region R) underscores the inherent sensitivity of the boundary description process; this is entirely analogous to the sensitivity of derivatives with respect to noise.

For these reasons, it often is appropriate to specify boundaries with a function B taking continuous values between zero and one. Such a function might be viewed as a probability boundary description but we do not explore that issue. Instead our main concerns are utility and ease of numerical computation.

To accommodate a continuous boundary function B, the Mumford–Shah functional could be recast as

$$E(u, B) = w_1 \int_\Omega (Au - g)^2 (1 - B)^2 + w_2 \int_\Omega \nabla u \cdot \nabla u (1 - B)^2 + \int_\Omega B^2 \tag{3}$$

where w_1 and w_2 are scalar weights. Here we have replaced the integrals over $\Omega\backslash K$ by integrals over Ω with integrands multiplied by $(1 - B)^2$, the idea being that since $B \approx 1$ is near K, the integration of terms times $(1 - B)^2$ over K is nearly zero. Similarly the boundary length integral has been replaced by the integral of B^2.

Manuscript received May 7, 1996; revised October 27, 1997. This work was supported by the Office of Naval Research under Grant N00014-96-1-0456. The associate editor coordinating the review of this manuscript and approving it for publication was Dr. Andrew F. Laine.

G. Hewer is with the Naval Air Warfare Center, China Lake, CA 93555 USA.

C. Kenney and B. S. Manjunath are with the Electrical and Computer Engineering Department, University of California, Santa Barbara, CA 93106 USA (e-mail: manj@ece.ucsb.edu).

Publisher Item Identifier S 1057-7149(98)06389-1.

The rest of this paper focuses on minimizing a wide class of objective functionals that includes (3) as well as functionals of the type considered by Geman and others. Aside from the simplifications that result from using a common theoretical framework to compare competing methods, the main contributions of this paper can be summarized as

1) A closed-form solution is derived for the optimal boundary function B associated with a given approximation function u. For the objective functions considered in this paper, $B = r/(1+r)$, where r is the residual of the objective function. For example, for the Mumford–Shah functional (3), $r = w_1(Au - g)^2 + w_2\nabla u \cdot \nabla u$. The explicit form of the boundary function can then be used to reduce the objective function to a form in which the minimization problem can be recast as an equivalent PDE.
2) The general framework used in this paper allows one to compare different objective functions of the Mumford–Shah or Geman type for least squares (L_2 norm) approximation or the total variation (L_1 norm) approach of Osher and Rudin [16], [17]. This is discussed in detail in Section III.
3) A numerical algorithm to minimize the objective function is outlined in Section V. This PDE descent method is significantly faster than the stochastic search algorithms previously used, and as the experimental results indicate, the results compare favorably with existing methods.
4) The extent of the boundary is influenced by the terms $(1 - B)^2$ and B^2 in the objective functional. One could also work with $(1 - B)^\gamma$ and B^γ for any value $\gamma > 1$. However, the case $\gamma = 2$ is sufficiently general because there is an equivalence between the case of arbitrary $\gamma > 1$ and the case $\gamma = 2$ with a modified residual function. This is discussed in Lemma 2 (Section IV) and the remarks following.

In the next section, we briefly review the related work in the literature, followed by a discussion of Mumford–Shah and Geman type objective functionals in Section III. In Section IV, we derive the formula for the optimal boundary function B and the reduced form of the objective functional. This is followed by a short description of the Euler–Lagrange variational procedure for determining the functional descent direction for the objective functional. The variational equations are most easily derived using the divergence theorem; this approach makes it clear that we should use Neumann boundary conditions for the descent PDE. This theoretical section is followed by a section devoted to numerical implementation and examples taken from synthetic and real images including satellite images and three-dimensional (3-D) medical computerized tomography (CT) images.

II. Relation to Related Work

There is a significant amount of related work in image processing and vision. Early work in this area dealt with scale space decompositions induced by Gaussian smoothing operators and the motion of edges (as identified with zero-crossings of the Laplacian) in scale space. See [10], [11], [22], [24], and [26].

Identifying spatial discontinuities is helpful in many applications such as segmentation, optical flow, stereo, and image reconstruction. The concept of a "line process" is useful in studying these problems as one of regularization. The binary line process was introduced by Geman and Geman [6] where the authors considered simulated annealing based algorithms for achieving the global optimization. Since then, several modifications of the original scheme have been suggested. Blake and Zisserman [4] formulated the same problem as minimizing an objective functional which enforces smoothness while eliminating the binary line process. See also Geiger and Gersosi [5], Geman and Reynolds [8], and Rangarajan and Chellappa [19]. Some of these recent works involve analog or continuous line processes. The connections between the line process approach to regularization and outlier processes in robust statistics is explored by Black and Rangarajan [3].

Common to all these algorithms is an objective functional that

1) enforces closeness to the original data by including terms such as $(u - g)^2$ or $(Au - g)^2$;
2) promotes local smoothness away from edges by including terms depending on $\|\nabla u\|$;
3) limits the extent of the boundary.

For example, Richardson [20] and Richardson and Mitter [21] consider minimizing functionals of the form

$$E_c(u, v) = \int_\Omega \beta(u - g)^2 + \Phi(v)\|\nabla u\|^2 + \alpha\left(c\Psi(v)\|\nabla v\|^2 + \frac{(1-v)^2}{4c}\right) \quad (4)$$

where α, β, and c are weighting factors and v is a continuous function describing the boundary. Ambrosio and Tortorelli [1], [2] have shown that, for $\Phi(v) = v^2$ and $\Psi(v) = 1$, this functional "Γ-converges" as $c \to 0$ to the following form of the Mumford–Shah functional

$$E(u, v) = \int_\Omega \beta(u - g)^2 + \int_{\Omega \setminus K} \|\nabla u\|^2 + \alpha|K| \quad (5)$$

where $|K|$ is the length of the boundary K.

In a similar vein, Shah [23] proposed minimizing a pair of functionals dependent on u and v: given u find v minimizing

$$V_u(v) = \int_\Omega \alpha(1 - v)^2\|\nabla u\| + \frac{\rho}{2}\|\nabla v\|^2 + \frac{v^2}{2\rho} \quad (6)$$

where α and ρ are weighting parameters. Given v find u minimizing

$$U_v(u) = \int_\Omega \|\nabla u\|^2 + \frac{(u - g)^2}{v^2\sigma^2} \quad (7)$$

where σ is a weighting parameter.

The idea of the second functional is that the boundary function v is approximately zero inside regions where we want $u - g$ to be small. Hence, the division of $(u - g)^2$ by v^2 can be interpreted as a local weighting that enforces close approximation of g inside regions. Applying a steepest decent

minimization procedure to these functionals yields a pair of coupled diffusion PDE's for u and v. This is also the case for the functionals studied by Richardson and Mitter.

However, as noted by Proesmans *et al.* [18], Shah's approach leads to blurring of the edges; this can be partially offset by working with a modified objective functional, in which the term $(u-g)^2/v^2\sigma^2$ replaced by $((u-g)^2/\sigma^2)(1-v)^2$, but some blurring still remains.

This blurring effect appears to be induced in part by the inclusion of the boundary gradient term $||\nabla v||$ in the objective functional, since this results in a diffusion PDE for v. Inclusion of the boundary gradient term also has the effect of "masking" the boundary. That is, for a given approximation function u the optimal boundary function v is the solution of a nonlinear elliptic PDE and cannot be given explicitly.

In contrast, the objective functionals of the Mumford–Shah type (3) as well as objective functionals of the type considered by Geman and Reynolds [8], which extend the work of Geman *et al.* [7], do not include a boundary gradient term.

III. A General Framework for Reducible Objective Functionals

Consider the following generalized form of the Mumford–Shah functional (3):

$$E(u, B) = \int_\Omega r(1-B)^2 + \int_\Omega B^2 \tag{8}$$

where the residual term r depends on $Au-g$ as well as ∇u. For our purposes we have found the following form of r to be most useful

$$r = w_1(Au-g)^2 + w_2||\nabla u|| \tag{9}$$

but more general forms of r are also considered below. Functionals of this type have the big advantage that the optimal boundary function B can be found explicitly for any nonnegative residual function r: independent of the form of r we show that, for a given function u, the function B that minimizes $E(u, B)$ is given by

$$B = \frac{r}{1+r}. \tag{10}$$

We denote this optimal boundary function by $B = B(u)$. This allows us to eliminate B from the objective functional and (after some simple algebra) we are led to the equivalent problem of minimizing the functional $E(u) \equiv E(u, B(u))$

$$E(u) = \int_\Omega \frac{r}{1+r}. \tag{11}$$

It is interesting that this reduced functional is equal to the L_1 norm of the optimal boundary function B; that is minimization of the reduced functional is really the same as minimizing the L_1 norm of B subject to $B = r/(1+r)$.

A. Geman Type Functionals

A similar reduction procedure is possible with functionals of the type considered by Geman and others [6]–[8].

In [8], Geman and Reynolds looked at objective functionals depending only on the approximation function u of the form

$$H(u) = \sum_S \lambda(Au-g)^2 + \sum_C \phi(D_C(u)/\Delta) \tag{12}$$

where λ and Δ are weights, S is the set of pixels indices, C is the set of "cliques" (or neighboring pixels), D_C is a difference function akin to a directional gradient, and ϕ is a specified function. For example, in [8], Geman and Reynolds used

$$\phi(x) = \frac{-1}{1+|x|} \tag{13}$$

since this function was empirically noted to have "yielded consistently good results."

The functional (12) was shown by Geman and Reynolds to be associated with a dual functional of the form

$$H^*(u, b) = \sum_S \lambda(Au-g)^2 + \sum_C b(D_C(u)/\Delta)^2 + \psi(b) \tag{14}$$

provided that the functions ϕ and ψ satisfy $\phi(x) = \inf_{0\le b}(bx^2 + \psi(b))$. The association of the two functionals arises from the fact that, for a given approximation u, the optimal boundary function $b = b(u)$ can be found explicitly. Substituting this value of b into H^* eliminates the b dependence and yields the functional H:

$$H^*(u, b(u)) = H(u). \tag{15}$$

We can recast the Geman type functionals in the form

$$G(u, B) = \int_\Omega w_1(Au-g)^2 + \int_\Omega w_2||\nabla u||(1-B)^2 + \int_\Omega B^2. \tag{16}$$

As in the case of the Mumford–Shah functionals, the optimal boundary function $B = B(u)$ (for a given u) for this functional can be found explicitly:

$$B = \frac{r}{1+r} \tag{17}$$

with $r = w_2||\nabla u||$.

The connection between this functional and those considered in [8] can be seen by substituting $B = B(u)$ into G to get

$$\begin{aligned} G(u, B(u)) &= \int_\Omega w_1(Au-g)^2 + \int_\Omega \frac{w_2||\nabla u||}{1+w_2||\nabla u||} \\ &= \int_\Omega w_1(Au-g)^2 + \int_\Omega 1 - \frac{1}{1+w_2||\nabla u||} \\ &= \int_\Omega w_1(Au-g)^2 + \int_\Omega \frac{-1}{1+w_2||\nabla u||} + C \\ &= \int_\Omega w_1(Au-g)^2 + \int_\Omega \phi(w_2||\nabla u||) + C \end{aligned}$$

where the constant C is equal to $\int_\Omega 1$ and $\phi(x) = -1/(1+|x|)$. Thus, this functional differs only by a constant from the integral form of the Geman and Reynolds functional (12) for the choice $\phi(x) = -1/(1+|x|)$. (Note the slight difference however in that our reformulation of the Geman functional

uses ∇u to measure approximation smoothness rather than separate terms for $\partial u/\partial x$ and $\partial u/\partial y$. While it is possible to retain these separate terms in a reformulation, we have avoided doing so since they introduce a directional bias, as seen by the numerical examples.)

Explicit formulas for the optimal boundary term make it easier to gain insight into the expected behavior of the segmentation algorithm. For example, the optimal boundary functions for the Mumford–Shah functional (8) and the Geman functional (12) are both given by $B = r/(1+r)$ where

$$\begin{aligned} r_{\mathrm{MS}} &= w_1(Au-g)^2 + w_2\|\nabla u\| && \text{Mumford–Shah} \\ r_{\mathrm{G}} &= w_2\|\nabla u\| && \text{Geman.} \end{aligned}$$

From this we see that the Geman optimal boundary function does not include the approximation error term $(Au-g)^2$. That is, it derives all of its boundary information from the gradient of the approximation function u. Since the term $(Au-g)^2$ measures the "residual noise" in the approximation we expect the that Geman boundary function should be smoother than the Mumford–Shah boundary function. We also see that, for the same function u and the same gradient weight w_2, the Mumford–Shah residual r_{MS} is larger than the Geman residual r_{G}. Consequently, $B_{\mathrm{MS}} \geq B_{\mathrm{G}}$.

However, the increased smoothness of B_{G} over B_{MS} and the inequality $B_{\mathrm{MS}} \geq B_{\mathrm{G}}$ assumes that the same approximation u is used in determining r_{MS} and r_{G}. In general, it is not the case that the optimal approximation function u is the same for the Mumford–Shah and Geman functionals.

B. Other Residual Functions

In the section on numerical results we return to the question of comparing Mumford–Shah and Geman type segmentation schemes for more general residual functions based on arbitrary L_p norms, especially L_1 and L_2 norms. For example, for the Mumford–Shah functionals we consider the following residual:

$$r = w_1((Au-g)^2+\delta)^{p_1/2} + w_2(\nabla u \cdot \nabla u + \delta)^{p_2/2} \quad (18)$$

where we assume δ is some small positive number. (We need $\delta > 0$ to ensure that r is differentiable at $Au - g = 0$ for $p_1 = 1$ or $\nabla u = 0$ for $p_2 = 1$.) In the numerical experiments we look at results for the $L_{2,2}$ residual ($p_1 = p_2 = 2$) and the mixed $L_{2,1}$ residual ($p_1 = 2$ and $p_2 = 1$). The $L_{2,2}$ residual corresponds to the usual least squares residual and tends to give overly smooth results and ringing near the boundary. The $L_{2,1}$ residual has the form of (9) and is better at preserving sharp edges. This choice of residual is closely related to the total variation methods of Osher and Rudin [16], [17] who obtained excellent results for image restoration using total variation methods (without the use of boundary functions) based on objective functions with L_1 norms.

The possibility of multichannel image information leads us to another type of residual function. For example, we may have multiple images $g_1, g_2, \cdots, g_k$ of the same object. Such a sequence could also be obtained from multispectral imaging or from a multiresolution decomposition of one original image. Given $g_1, g_2, \cdots, g_k$ we can define the multichannel L_{p_1,p_2} residual function

$$r = \sum_{i=1}^{k} w_1((Au_i - g_i)^2+\delta)^{p_1/2} + w_2(\nabla u_i \cdot \nabla u_i + \delta)^{p_2/2}. \quad (19)$$

IV. The Optimal Boundary Function

Given an image g and an approximation function u, the following lemma shows that there is a unique boundary function that minimizes $E(u, B)$.

Lemma 1: Let $r = r(u, g, \nabla u)$ be nonnegative. For fixed g and u, the objective functional defined by

$$E(u, B) = \int_\Omega r(1-B)^2 + \int_\Omega B^2 \quad (20)$$

is minimized by setting $B = r/(1+r)$. Moreover, for any B

$$E(u, B) \geq \int_\Omega \frac{r}{1+r} \quad (21)$$

with equality only for $B = r/(1+r)$.

Proof: For any B

$$\begin{aligned} r(1-B)^2 + B^2 &= (1+r)B^2 - 2rB + r \\ &= (1+r)\left(B - \frac{r}{1+r}\right)^2 + \frac{r}{1+r} \\ &\geq \frac{r}{1+r} \end{aligned}$$

with equality for $B = r/(1+r)$ which completes the proof.

The next lemma shows that the freedom to choose the form of the residual function r means that there is an equivalence between the choice of $\gamma = 2$, as the exponent of $(1-B)$ and B in the objective functional, and the case of arbitrary $\gamma > 1$.

Lemma 2: Assume that γ is greater than one. Let $r = r(u, g, \nabla u)$ be nonnegative. For fixed g and u, the objective functional

$$E(u, B, \gamma) = \int_\Omega r|1-B|^\gamma + \int_\Omega |B|^\gamma \quad (22)$$

is minimized by the setting $B = \rho/(1+\rho)$ where $\rho = r^{1/(\gamma-1)}$. Moreover, for any B

$$E(u, B, \gamma) \geq \int_\Omega \left(\frac{\rho}{1+\rho}\right)^{\gamma-1} \quad (23)$$

with equality only for $B = \rho/(1+\rho)$.

Proof: Thus $E(u, B, \gamma)$ is minimized by selecting B as the minimizer of $f(r, B) = r(1-B)^\gamma + B^\gamma$. For $\gamma > 1$, the function f is convex in $B \in (0, 1)$ since $d^2f/dB^2 = \gamma(\gamma-1)(r(1-B)^{\gamma-2} + B^{\gamma-2}) > 0$. Moreover, $df/dB = \gamma(B^{\gamma 1} - r(1-B)^{\gamma-1})$ is negative or zero at $B = 0$ and positive at $B = 1$. Thus $f(r, \cdot)$ has a unique minimizer B_γ that lies in the interval $0 \leq B_\gamma < 1$. Setting $df/dB = 0$ and solving for B gives

$$B = \frac{r^{\gamma-1}}{1+r^{\gamma-1}}. \quad (24)$$

Substituting this value into $E(u, B, \gamma)$ gives, with $B(u) \equiv \rho/(1+\rho)$

$$E(u, \gamma) = \int_\Omega \left(\frac{\rho}{1+\rho}\right)^{\gamma-1} \tag{25}$$

which completes the proof since $B = B(u)$ minimizes $E(u, B, \gamma)$.

Remark: It is interesting to note that this reduced functional is equal to $||B(u)||_{\gamma-1}^{\gamma-1}$; that is minimization of the reduced gamma-functional is really the same as minimizing the $L_{\gamma-1}$ norm of B subject to $B = \rho/(1+\rho)$ where $\rho = r^{1/(\gamma-1)}$.

We also are in a position to address the question of equivalence between the case $\gamma = 2$ and arbitrary $\gamma > 1$. That is, can we obtain equality in the reduced objective functionals by the proper choice of residual functions? Let r_2 and r_γ denote the residual functions for $\gamma = 2$ and arbitrary $\gamma > 1$. By Lemma 1, the objective functional

$$E(u, B) = \int_\Omega r_2(1-B)^2 + \int_\Omega B^2 \tag{26}$$

has the reduced functional (after substituting in the optimal boundary function B)

$$E(u) = \int_\Omega \frac{r_2}{1+r_2}. \tag{27}$$

By Lemma 2, the objective functional

$$E(u, B, \gamma) = \int_\Omega r_\gamma(1-B)^\gamma + \int_\Omega B^\gamma \tag{28}$$

has the reduced functional

$$E(u, \gamma) = \int_\Omega \left(\frac{\rho}{1+\rho}\right)^{\gamma-1} \tag{29}$$

where $\rho = r_\gamma^{1/(\gamma-1)}$.

Thus, we see that $E(u)$ is equal to $E(u, \gamma)$ if

$$\frac{r_2}{1+r_2} = \left(\frac{\rho}{1+\rho}\right)^{\gamma-1} \tag{30}$$

where $\rho = r_\gamma^{1/(\gamma-1)}$. Solving for r_2 we find

$$r_2 = \frac{\left(\frac{\rho}{1+\rho}\right)^{\gamma-1}}{1-\left(\frac{\rho}{1+\rho}\right)^{\gamma-1}}. \tag{31}$$

From this we conclude that by exploiting our freedom to choose the form of r as a function of g, u and ∇u, we may work entirely with the case $\gamma = 2$.

We conclude this section with the analog of Lemma 1 for Geman functionals.

Lemma 3: Let $r_i = r_i(u, g, \nabla u)$ be nonnegative for $i = 1, 2$. For fixed g and u, the objective functional defined by

$$E(u, B) = \int_\Omega r_1 + \int_\Omega r_2(1-B)^2 + \int_\Omega B^2 \tag{32}$$

is minimized by setting $B = r_2/(1+r_2)$. Moreover, for any B

$$E(u, B) \geq \int_\Omega r_1 + \int_\Omega \frac{r_2}{1+r_2} \tag{33}$$

with equality only for $B = r_2/(1+r_2)$.

Proof: The proof is exactly the same as for Lemma 1.

As per Lemma 2, the choice of 2 as an exponent on $(1-B)$ and B in the Geman functional is sufficiently general to capture the behavior of arbitrary $\gamma > 1$ by modifying the residual function. For brevity we omit the details.

V. Numerical Implementation

The previous sections discussed various functionals for approximating and segmenting images. These functionals contain terms related to the approximation error and the smoothness of the approximation as well as the extent of the boundary. Once the form of the functional has been selected, the nontrivial problem of finding the minimizing approximation u has to be addressed. Typically, the desired approximation is an equilibrium solution of a nonlinear diffusion PDE with certain boundary conditions. A general procedure for finding these PDE's is outlined in the Appendix but we indicate the main ideas and results in this section.

To illustrate, suppose that we wanted to minimize a functional of the form

$$E(g, u) = \int_\Omega (u-g)^2 + \int_\Omega \nabla u \cdot \nabla u \tag{34}$$

where g is the given image and u is an approximation of g.

The minimizing approximation u for this functional satisfies the ellpitic equilibrium PDE

$$\begin{aligned} \triangle u &= u - g \\ \partial u/\partial n &= 0 \qquad \text{on } \partial\Omega \end{aligned}$$

where $\triangle u$ is the Laplacian of u and $\partial u/\partial n$ denotes the normal derivative.

Numerically, we can either solve for the equilibrium solution directly or follow u as a function of t from an initial approximation, such as $u_0 = g$, by integrating the diffusion PDE

$$u_t = g - u + \triangle u \tag{35}$$

subject to the Neumann boundary condition

$$\frac{\partial u}{\partial n} = 0 \qquad \text{on } \partial\Omega. \tag{36}$$

Starting from the initial condition u_0 the image u evolves as $t \to \infty$ toward the equilibrium solution.

The following theorem gives a similar treatment for the reduced form of the Mumford–Shah functional, $E(g, u) = \int r/(1+r)$, where the residual function r has the form

$$r = r((Au-g)^2, \nabla u \cdot \nabla u). \tag{37}$$

As a matter of notation, we refer to the first and second arguments of r as $z_1 = (Au-g)^2$ and $z_2 = \nabla u \cdot \nabla u$, respectively.

Theorem 1: Let $E(g, u) = \int_\Omega r/(1+r)$. Given an initial approximation u_0 defined over $x \in \Omega$ with $\partial u_0/\partial n = 0$ on $\partial\Omega$, let $u = u(x, t)$ satisfy

$$u_t = A^T\left(\frac{(g-Au)}{(1+r)^2}\frac{\partial r}{\partial z_1}\right) + \nabla\cdot\left(\frac{\nabla u}{(1+r)^2}\frac{\partial r}{\partial z_2}\right) \quad (38)$$

subject to

$$u(x, 0) = u_0, \qquad \text{for } x \in \Omega$$
$$\partial u/\partial n = 0, \qquad \text{for } x \in \partial\Omega.$$

Then $E(g, u(\cdot, t))$ is a decreasing function of t unless u_t is identically zero in which case $E(g, u(\cdot, t))$ is constant.

Proof: See the Appendix.

For the reduced form of the Geman functional we have the following result.

Theorem 2: Let $G(g, u) = \int_\Omega r_1 + \int_\Omega r_2/(1+r_2)$ where r_1 is a nonnegative function of $z_1 = (Au-g)^2$ and r_2 is a nonnegative function of $z_2 = \nabla u \cdot \nabla u$.

Given an initial approximation u_0 defined over $x \in \Omega$ with $\partial u_0/\partial n = 0$ on $\partial\Omega$, let $u = u(x, t)$ satisfy

$$u_t = A^T\left((g-Au)\frac{\partial r_1}{\partial z_1}\right) + \nabla\cdot\left(\frac{\nabla u}{(1+r_2)^2}\frac{\partial r_2}{\partial z_2}\right) \quad (39)$$

subject to

$$u(x, 0) = u_0, \qquad \text{for } x \in \Omega$$
$$\partial u/\partial n = 0, \qquad \text{for } x \in \partial\Omega.$$

Then $G(g, u(\cdot, t))$ is a decreasing function of t unless u_t is identically 0 in which case $G(g, u(\cdot, t))$ is constant.

Proof: See the Appendix.

Once we have defined a residual function and obtained the corresponding PDE for u, we then use Euler's method to integrate the descent PDE and halt the integration when the decrease in the value of the objective functional becomes less than a user supplied tolerance. Typically, we obtained good results by stopping when the decrease in the objective functional from one Euler step to the next was less than 1% of the current value of the objective functional.

The step size for Euler's method was determined in the following way. Let v_0 denote the value of the objective functional at the initial image approximation u_0. (For our experiments we set $u_0 = g$.) Starting with a nominal stepsize $dt = 1$, the value v_1 of the objective functional for the updated image $u_1 = u_0 + dt * u_t$ was computed. We then checked to see if the value of the objective functional was smaller for u_1 than for u_0. If not, the stepsize was cut in half. To be sure the stepsize was really acceptable, we continued to cut the stepsize in half until the condition $v_0 > v_1$ had been satisfied several times in a row (usually three or four times).

This PDE descent procedure may only lead to a local minimum for the objective functional. Other methods, such as simulated annealing, can be used to find a global minimum for the objective functional with high probability, but the intensive computational costs may result in unacceptably long processing times. For the examples we tested, the choice of $u_0 = g$ produced excellent results for the PDE descent method with only short processing times.

VI. Experimental Results

A. Synthetic Images

The following examples are designed to show the effects of varying the parameters and residual forms of the objective functions discussed in the previous sections.

Example 1: The Gaussian hump shown in Fig. 1(a) presents a smooth image with no discontinuities. Fig. 1(b) and (f) display the approximation function u and the associated boundary function B for the original Geman type functional with the smoothness of the approximation measured by $\partial u/\partial x$ and $\partial u/\partial y$ separately. As seen in these two figures, this introduces an x, y bias in an image that is originally circularly symmetric. This bias is eliminated, as seen in Fig. 1(c) and (g) by modifying the Geman functional to the form (16) so that the smoothness of the approximation function u is measured by the norm of the gradient of u, since this is independent of the coordinate orientation. In these images, we have used the total variation norms ($p_1 = 2, p_2 = 1$) for the functional in (57) and this results in a slight flattening effect at the center of the Gaussian hump. This flattening effect is not present if we use the least squares norms ($p_1 = 2, p_2 = 2$) in the Geman functional as seen in Fig. 1(d) and (h). We also note, however, that the total variation norms can avoid the flattening effect by increasing the approximation weight w_1. This is shown in Fig. 1(e) and (i) for $w_1 = 10$, $w_2 = 1$. For all the other results for this example we used $w_1 = 1$, $w_2 = 1$.

Example 2: Fig. 2(a) presents a piecewise constant image similar to an example considered by Richardson in [20]. Fig. 2(b) and (c) shows, respectively, the approximation function u and the boundary function b for the Mumford–Shah functional (50) with $w_1 = w_2 = 10$ and $p_1 = 2, p_2 = 1$. This total variation result compares well with the smoothing effect of the least squares result ($p_1 = p_2 = 2$) seen in Fig. 2(d) and (e). For this example the Geman functional results are nearly identical.

Example 3: This is the same as Example 2 but with Gaussian noise added as seen in Fig. 3(a). Fig. 3(b) and (c) shows, respectively, the approximation function u and the boundary function b for the Mumford–Shah functional with $w_1 = w_2 = 10$ and $p_1 = 2, p_2 = 1$. It is interesting that the associated Geman approximation function u for the same parameter choices is nearly identical as seen in Fig. 3(d), but the Geman boundary function B in Fig. 3(e) is not as noisy as the Mumford–Shah boundary function. See the remarks at the end of Section III-A for a discussion of this effect.

There is also another approach, involving iteration, that can be used to remove noise in both the approximation and the boundary function. In this approach, we start with an initial image g and use a segmentation scheme to generate an approximation u. In turn this approximation is used as an initial image to generate another approximation u_1, and we may repeat as often as desired with each successive approximation becoming smoother. This is illustrated in Fig. 3(f), which shows the first iterate u_1 for the noisy piecewise constant example image. Fig. 3(g) shows the associated boundary function which is almost entirely noise-free.

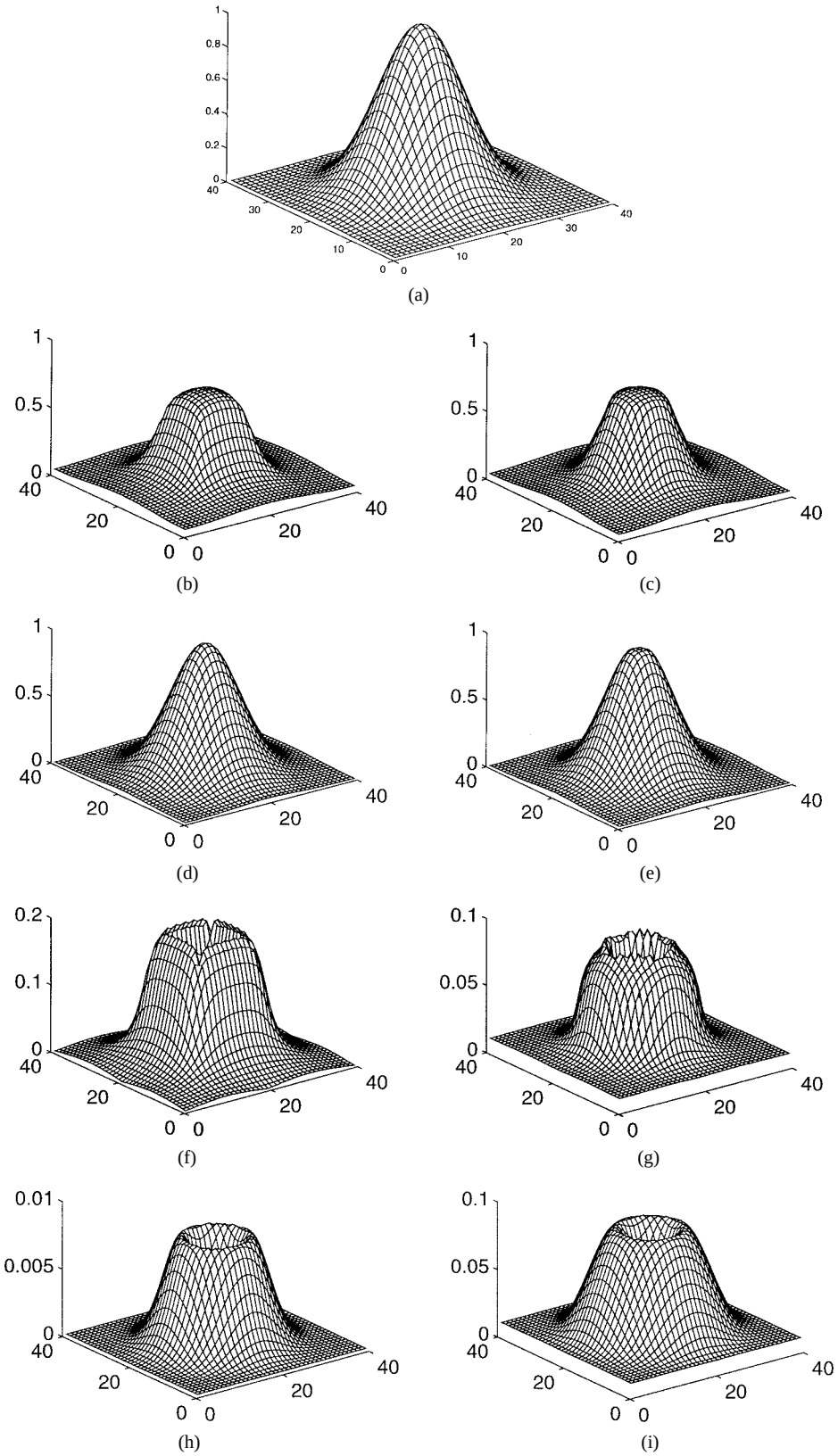

Fig. 1. (a) Gaussian hump. (b) and (c) Approximations for the Geman and modified Geman type functionals using the total variation norms. Note the flattening of the centers. Using a least-squares norm or increasing the approximation weight removes this flattening effect as shown in (d) and (e), respectively. The corresponding boundary functions are shown in (f)–(i).

B. Real Images

Experimental results on three different classes of real images are provided by the following examples. The results for these examples were obtained using the boundary function b for the Mumford–Shah functional (50) with $p_1 = 2, p_2 = 1$ for various weights as listed on next page.

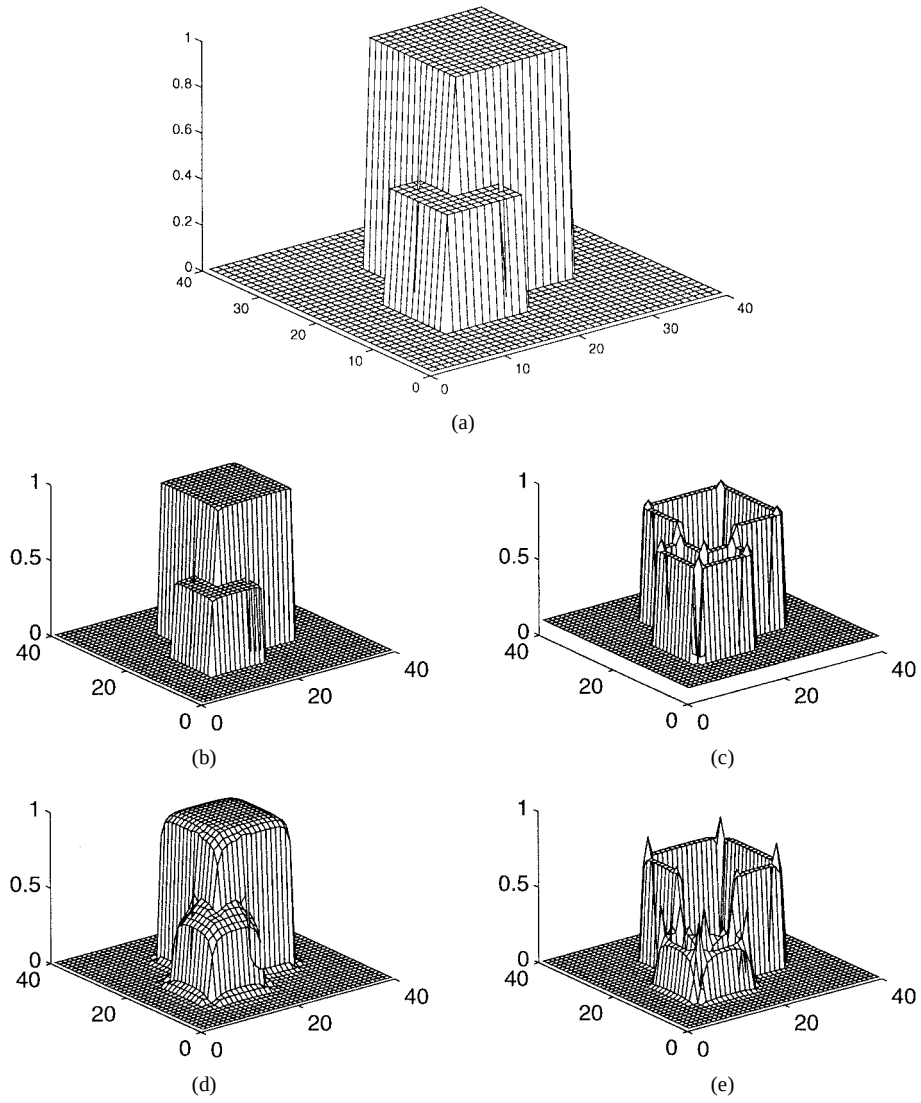

Fig. 2. (a) Piecewise constant image. (b)–(c) Approximation and boundary functions, respectively, for the Mumford–Shah functional. (d)–(e) Approximation and boundary functions for the Geman-type functional.

Example 4: Fig. 4 presents results on two face images with $w_1 = w_2 = 10$. The approximation functions u in the figures appear much like an artists' sketch. This simplification means that the approximations are more suitable for face feature extraction than the original images. We are currently using the approximation and boundary information in our work on face image tracking.

Example 5: An example of segmenting out kidney X-ray CT images is shown in Fig. 5. Here we used the weights $w_1 = 100, w2 = 10$. The proposed segmentation approach is used in identifying regions containing kidneys in these CT studies and to localize problems such as a cyst. Combined with simple domain specific heuristics, this approach provides a robust classification algorithm which is currently being incorporated into the development of a medical image data base system.

Example 6: Finally, an application to satellite image segmentation for use in image registration is shown in Fig. 6. Fig. 6(a) shows a LANDSAT image, boundary regions of a segment [Fig. 6(b)] of which are shown in Fig. 6(d). Fig. 6(c) shows the approximation image for $w_1 = w_2 = 10$. For comparison, Fig. 6(e) shows the boundaries detected using an algorithm based on Laplacian of the Gaussian filtering. The image is first convolved with the LoG filter and is followed by thresholding with hysteresis to detect strong contours. The details are described in [9], wherein it was used in multisensor image registration. Comparing Fig. 6(d) and (e), it is clear that the proposed objective functional minimization approach does produce boundaries consistent with the physical regions. In contrast, pure edge-detection-based algorithms tend to result in less reliable regions boundaries. Preliminary experiments indicate that the proposed approach produces more robust contours for image registration.

The results clearly demonstrate the suitability of the proposed method in diverse image processing applications.

VII. Conclusion

We have presented a general framework for segmenting images and obtaining region boundaries based on minimiz-

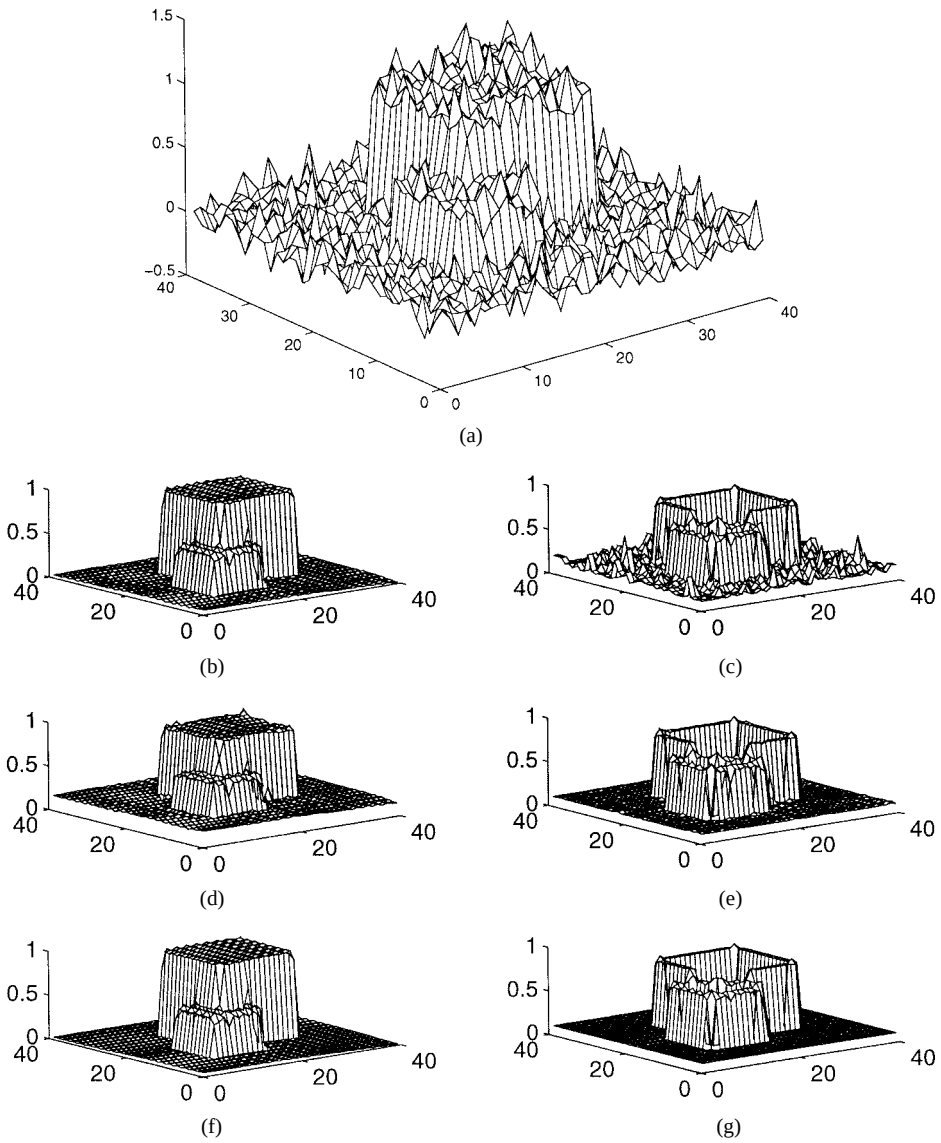

Fig. 3. (a)–(e) Same as Fig. 2 but with additive Gaussian noise. (f)–(g) Result of an iterative approach which uses (b) as the initial image. Note that the boundary function (g) is almost entirely noise free.

ing an objective functional for which the optimal boundary function has a particularly simple form. The explicit form of the boundary function in terms of the approximating function permits the reduction of the original objective function to a form that depends only on the approximation function. From this, a PDE descent procedure can be used to minimize the objective function. Many commonly used segmentation approaches such as the Mumford–Shah method and Geman type schemes can be represented in this framework, which is also general enough to include least squares and total variation forms. The explicit form of the boundary function also allows some analytic comparison between competing methods. Although excellent numerical results have been obtained on a wide variety of real and synthetic images, further research is needed on the problem of selecting the best weights for a given image or class of images, as well the problem of automatically selecting the best choice of norms for the residual function.

APPENDIX

Given g and u we want to know how to change u so as to decrease the value of the reduced Mumford–Shah functional $E(g, u) = \int r/(1 + r)$ or the reduced Geman function $E(g, u) = \int r_1 + \int r_2/(1 + r_2)$. The basic idea of the Euler–Lagrange variational procedure is to replace u by $u+\epsilon h$ where $\epsilon > 0$ is a small positive number and h is an arbitrary function. We then expand $E(g, u + \epsilon h)$ and seek conditions on h that ensure that $E(g, u + \epsilon h) \leq E(g, u)$. However, the expansion of $E(g, u + \epsilon h)$ involves a term with ∇h. We need to rework this term into an expression involving only h rather than ∇h. This is done by using the divergence theorem, which is the higher dimensional analog of the integration by parts formula.

To illustrate the procedure, suppose that we wanted to minimize a functional of the form

$$E(g, u) = \int_{\Omega} (u - g)^2 + \nabla u \cdot \nabla u. \tag{40}$$

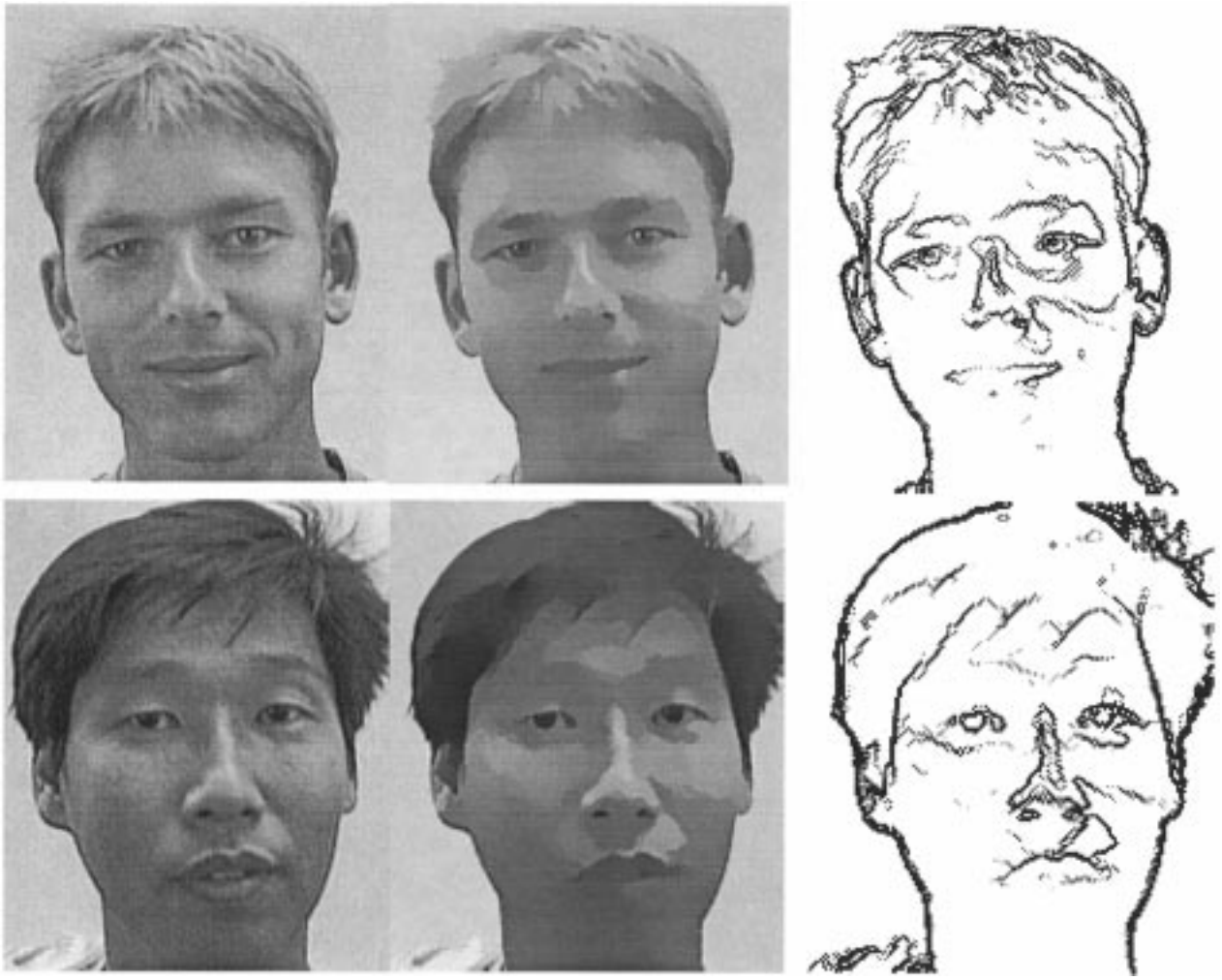

Fig. 4. Smoothing face images. Original images are on the left, the approximations are in the middle, and the boundary functions are shown on the right.

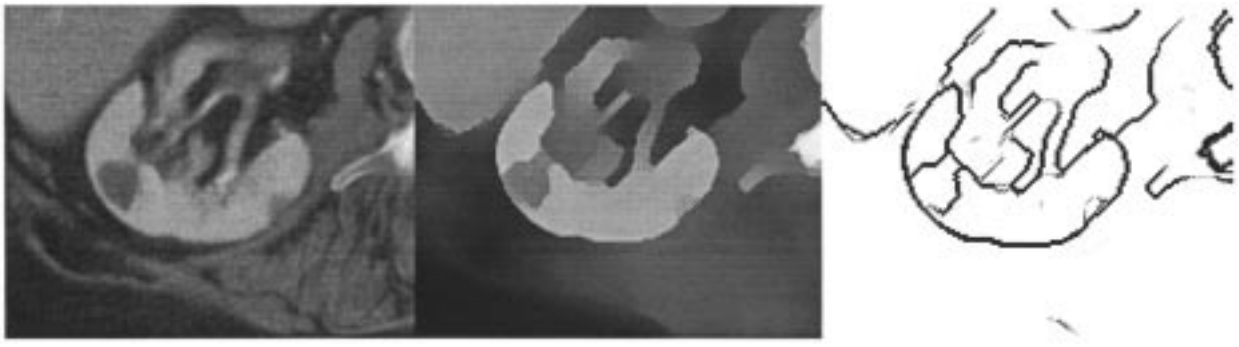

(a) (b) (c)

Fig. 5. X-ray kidney CT image segmentation. (a) Original image. (b) Approximation. (c) Boundary function. Note that the cyst in the kidney (grey region inside the kidney) is clearly segmented.

Such a functional would arise if we were only interested in the problem of approximating g by a smooth function u, without regard to the boundary function. Now replace u by $u+\epsilon h$:

$$E(g,\, u+\epsilon h) = \int_\Omega (u+\epsilon h-g)^2 + \nabla(u+\epsilon h)\cdot\nabla(u+\epsilon h)$$
$$= \int_\Omega (u-g)^2 + \nabla u\cdot\nabla u$$
$$+ 2\epsilon\int_\Omega (u-g)h + \nabla u\cdot\nabla h + O(\epsilon^2)$$
$$= E(g,\, u) + 2\epsilon\int_\Omega (u-g)h + \nabla u\cdot\nabla h + O(\epsilon^2).$$

By the divergence theorem (see below)

$$\int_\Omega \nabla u\cdot\nabla h = -\int_\Omega h\triangle u + \int_{\partial\Omega} h\partial u/\partial n \qquad (41)$$

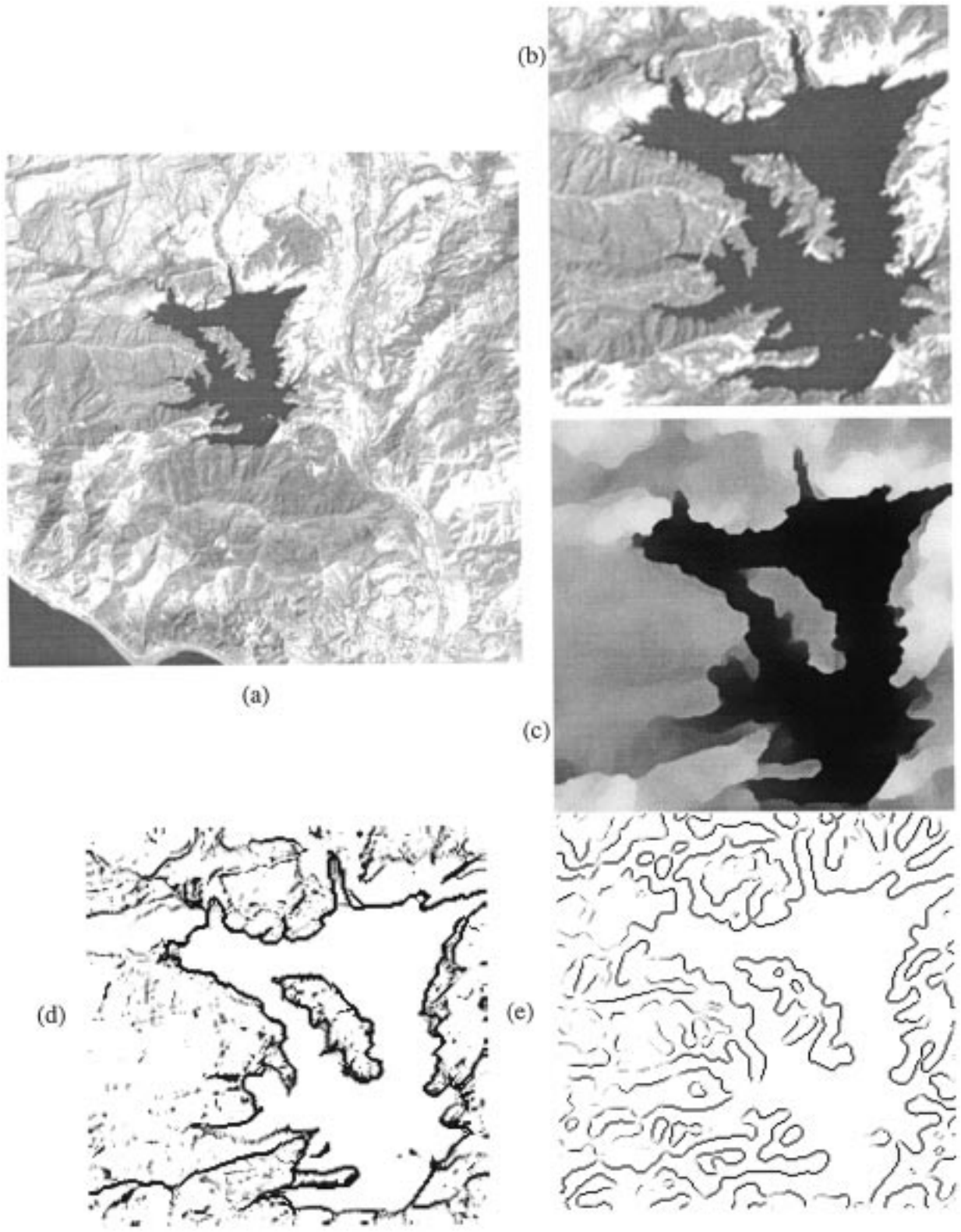

Fig. 6. (a) LANDSAT image, (b) segment around the lake, (c) approximation, (d) boundary function, and (e) edges detected using a contour detection algorithm used for registration applications are shown for comparison.

where $\triangle u$ is the Laplacian of u and $\partial u/\partial n$ is the normal derivative of u on the boundary of Ω. If we assume that u satisfies the Neumann boundary condition $\partial u/\partial n = 0$, then

$$\int_\Omega \nabla u \cdot \nabla h = -\int_\Omega h \triangle u. \tag{42}$$

Substituting this into the expansion of $E(g, u+\epsilon h)$ gives

$$E(g, u+\epsilon h) = E(g, u) + 2\epsilon \int_\Omega ((u-g) - \triangle u)h + O(\epsilon^2).$$

Thus, we can force the objective functional to decrease by

setting

$$h = -((u - g) - \triangle u) \tag{43}$$

and taking $\epsilon > 0$ sufficiently small. Identifying h with u_t gives the descent PDE

$$u_t = g - u + \triangle u \tag{44}$$

subject to the Neumann boundary condition

$$\frac{\partial u}{\partial n} = 0, \qquad \text{on } \partial\Omega. \tag{45}$$

Starting from the initial condition $u(x, y, 0) = g(x, y)$ the image u evolves toward the equilibrium solution to

$$\begin{aligned} \triangle u &= u - g \\ \partial u/\partial n &= 0, \qquad \text{on } \partial\Omega. \end{aligned}$$

Numerically, we can either solve for the equilibrium solution directly or follow u as a function of t from its initial condition $u = g$ by using the Euler update formula $u_{n+1} = u_n + dtu_t$ where dt is the Euler stepsize.

Of course for our purposes we want to include the boundary function B in the objective function. This results in a different descent PDE, but the basic procedure for determining the descent PDE is the same as above.

A. The Divergence Theorem

For a smooth vector valued function $F = (F_1, F_2, \cdots, F_n)$ the divergence of F is defined by

$$\nabla \cdot F = \frac{\partial F_1}{\partial x_1} + \frac{\partial F_2}{\partial x_2} + \cdots + \frac{\partial F_n}{\partial x_n}. \tag{46}$$

Assuming that F is smooth over Ω and the boundary $\partial\Omega$, the divergence of F inside Ω is related to the flow of F across the boundary $\partial\Omega$:

$$\int_\Omega \nabla \cdot F = \int_{\partial\Omega} F \cdot n \tag{47}$$

where $n = n(x)$ is the outward unit normal at $x \in \partial\Omega$. See Warner [25, p. 151]. For the purposes of instruction, this formula is often referred to as the "conservation of dots and dels."

We need to transform integral expressions involving $q\nabla h \cdot \nabla u$, where q, h, and u are functions, into integral expressions involving h and derivatives of q and u.

Lemma 4: If $\nabla u \cdot n = 0$ on the boundary of Ω then

$$\int_\Omega q\nabla h \cdot \nabla u = -\int_\Omega h\nabla \cdot (q\nabla u). \tag{48}$$

Proof: To prove (48) use the divergence theorem with $F = qh\nabla u$. Since $\nabla u \cdot n = 0$ on $\partial\Omega$ we have

$$\begin{aligned} 0 &= \int_{\partial\Omega} qh\nabla u \cdot n \\ &= \int_\Omega \nabla \cdot (qh\nabla u) \\ &= \int_\Omega q\nabla h \cdot \nabla u + \int_\Omega h\nabla \cdot (q\nabla u). \end{aligned}$$

B. Descent PDE's for the Mumford–Shah and Geman Functionals

In order to find the functional descent PDE for $E(g, u) = \int r/(1 + r)$ we will limit our discussion to residual functions of the form

$$r = r((Au - g)^2, \nabla u \cdot \nabla u). \tag{49}$$

However, the same basic technique works for more general residual functions.

As a matter of notation, we refer to the first and second arguments of r as $z_1 = (Au - g)^2$ and $z_2 = \nabla u \cdot \nabla u$, respectively. For example, setting

$$r(z_1, z_2) = w_1(z_1 + \delta)^{p_1/2} + w_2(z_2 + \delta)^{p_2/2} \tag{50}$$

gives the residual function

$$\begin{aligned} &r((Au - g)^2, \nabla u \cdot \nabla u) \\ &\quad = w_1((Au - g)^2 + \delta)^{p_1/2} + w_2(\nabla u \cdot \nabla u + \delta)^{p_2/2}. \end{aligned} \tag{51}$$

Proof of Theorem 1: In the statement of Theorem 1, the transpose A^T of the smoothing operator A is defined implicitly by the requirement that $\int_\Omega f_1 A f_2 = \int_\Omega f_2 A^T f_1$ for arbitrary functions f_1 and f_2. Application of the divergence theorem gives

$$\begin{aligned} \left.\frac{\partial E(g, u + \epsilon h)}{\partial \epsilon}\right|_{\epsilon=0} = \int_\Omega \Bigg(& A^T\left(\frac{2(Au - g)}{(1 + r)^2}\,\frac{\partial r}{\partial z_1}\right) \\ & -2\nabla \cdot \left(\frac{\nabla u}{(1 + r)^2}\,\frac{\partial r}{\partial z_2}\right)\Bigg) h. \end{aligned} \tag{52}$$

Thus setting $h = u_t$ as above ensures that $\partial E(g, u(\cdot, t))/\partial t \leq 0$ with equality only if u_t is identically zero over Ω, which completes the proof.

As an illustration, if

$$\begin{aligned} &r((Au - g)^2, \nabla u \cdot \nabla u) \\ &\quad = w_1((Au - g)^2 + \delta)^{p_1/2} + w_2(\nabla u \cdot \nabla u + \delta)^{p_2/2} \end{aligned} \tag{53}$$

then the descent PDE is given by

$$\begin{aligned} u_t = & A^T\left(\frac{p_1 w_1 (g - Au)}{(1 + r)^2}\left((Au - g)^2 + \delta\right)^{p_1/2-1}\right) \\ & + p_2 w_2 \nabla \cdot \left(\frac{\nabla u}{(1 + r)^2}\left(\nabla u \cdot \nabla u + \delta\right)^{p_2/2-1}\right). \end{aligned} \tag{54}$$

As a second illustration, in the multichannel case we might use the residual function

$$R = \sum_{i=1}^{k} r((Au_i - g_i)^2, \nabla u_i \cdot \nabla u_i) \tag{55}$$

where r is the $L_{p_1} - L_{p_2}$ residual given above in which case we have a system of k first-order descent PDE's:

$$\begin{aligned} (u_i)_t = & A^T\left(\frac{p_1 w_1 (g_i - Au_i)}{(1 + R)^2}\left((Au_i - g_i)^2 + \delta\right)^{p_1/2-1}\right) \\ & + p_2 w_2 \nabla \cdot \left(\frac{\nabla u_i}{(1 + R)^2}\left(\nabla u_i \cdot \nabla u_i + \delta\right)^{p_2/2-1}\right). \end{aligned} \tag{56}$$

The same approach yields the descent PDE for the Geman functional.

Proof of Theorem 2: The proof is basically the same as that for Theorem 1.

As an illustration, if

$$G(g, u) = \int_\Omega r_1 + \int_\Omega r_2/(1+r_2) \tag{57}$$

where

$$r_1((Au-g)^2) = w_1((Au-g)^2+\delta)^{p_1/2}$$
$$r_2(\nabla u \cdot \nabla u) = w_2(\nabla u \cdot \nabla u + \delta)^{p_2/2}$$

then the Geman descent PDE is given by

$$u_t = A^T(p_1 w_1(g-Au)((Au-g)^2+\delta)^{p_1/2-1}) + p_2 w_2 \nabla \cdot \left(\frac{\nabla u}{(1+r_2)^2}(\nabla u \cdot \nabla u + \delta)^{p_2/2-1}\right). \tag{58}$$

ACKNOWLEDGMENT

The authors would like to thank R. Schyoen (see Fig. 4) and Y. Deng for carrying out the simulations on the face and satellite images.

REFERENCES

[1] L. Ambrosio and V. Tortorelli, "On the approximation of functionals depending on jumps by elliptic functionals," *Commun. Pure Appl. Math.*, vol. 43, pp. 999–1036.
[2] ———, "Approximation of functionals depending on jumps by elliptic functionals via Γ-convergence," *Boll. Un. Mat. Ital.*, vol. 7, pp. 105–123, 1992.
[3] M. J. Black and A. Rangarajan, "The outlier process: Unifying line processes and robust statistics," in *Proc. IEEE Conf. Computer Vision and Pattern Recognition*, Seattle, WA, June 1994, pp. 15–22.
[4] A. Blake and A. Zisserman, *Visual Reconstruction.* Cambridge, MA: MIT Press, 1987.
[5] D. Geiger and F. Girosi, "Parallel and deterministic algorithms from MRFs: Surface reconstruction," *IEEE Trans. Pattern Anal. Machine Intell.*, vol. 13, pp. 401–412, May 1991.
[6] S. Geman and D. Geman, "Stochastic relaxation, Gibbs distributions, and Bayesian restoration of images," *IEEE Trans. Pattern Anal. Machine Intell.*, vol. PAMI-6, pp. 721–741, 1984.
[7] D. Geman, S. Geman, C. Graffigne, and P. Dong, "Boundary detection by constrained optimization," *IEEE Trans. Pattern Anal. Machine Intell.*, vol. 12, pp. 609–628, 1990.
[8] D. Geman and G. Reynolds, "Constrained restoration and the recovery of discontinuities," *IEEE Trans. Pattern Anal. Mach. Intell.*, vol. 14, pp. 376–383, Mar. 1992.
[9] H. Li, B. S. Manjunath, and S. K. Mitra, "A contour based approach to multisensor image registration," *IEEE Trans. Image Processing*, vol. 57, pp. 235–245, 1995.
[10] D. Marr and E. Hildreth, "Theory of edge detection," in *Proc. R. Soc. Lond. B*, 1980, vol. 207, pp. 187–217.
[11] D. Marr, *Vision.* Freeman and Co., 1980.
[12] J. Morel and S. Solimini, *Variational Methods in Image Segmentation.* Boston, MA: Birkhäuser, 1995.
[13] D. Mumford and J. Shah, "Boundary detection by minimizing functionals," in *Proc. IEEE Conf. Computer Vision and Pattern Recognition*, San Francisco, CA, 1985.
[14] ———, "Boundary detection by minimizing functionals," in *Image Understanding*, S. Ullman and W. Richards, Eds. Norwood, NJ: Ablex, 1988.
[15] ———, "Optimal approximation by piecewise smooth functions and associated variational problems," *Commun. Pure Appl. Math.*, vol. XLII, pp. 577–685, 1989.
[16] S. Osher and L. Rudin, "Feature-oriented image enhancement using shock filters," *SIAM J. Numer. Anal.*, vol. 27, pp. 919–940, 1990.
[17] ———, "Shocks and other nonlinear filtering applied to image processing," in *Proc. SPIE Appl. Dig. Image Proc. XIV*, 1991, vol. 1567, pp. 414–430.
[18] M. Proesmans, E. Pauwels, and L. van Gool, "Coupled geometry-driven diffusion equations for low-level vision," in *Geometry-Driven Diffusion in Computer Vision*, B. M. ter Harr Romeny, Ed. Boston, MA: Kluwer, 1994, pp. 1991–228.
[19] A. Rangarajan and R. Chellappa, "A continuation method for image estimation using the adiabatic approximation," in *Markov Random Fields: Theory and Applications*, R. Chellappa and A. K. Jain, Eds. New York: Academic, 1993.
[20] T. J. Richardson, "Scale independent piecewise smooth segmentation of images via variational methods," Ph.D. thesis, Mass. Inst. Technol., Cambridge, Feb. 1990.
[21] T. Richardson and S. Mitter, "Approximation, computation and distortion in the variational formulation," in *Geometry-Driven Diffusion in Computer Vision*, B. M. ter Harr Romeny, Ed. Boston, MA: Kluwer, 1994, pp. 169–190.
[22] A. Rosenfeld and M. Thurston, "Edge and curve detection for visual scene analysis," *IEEE Trans. Comput.*, vol. C-20, pp. 562–569, 1971.
[23] J. Shah, "Segmentation by nonlinear diffusion," in *Proc. Conf. Computer Vision and Pattern Recognition*, June 1991, pp. 202–207.
[24] A. Yuille and T. Poggio, "Scaling theorems for zero-crossings," *IEEE Trans. Pattern Anal. Machine Intell.*, vol. PAMI-8, pp. 15–25, 1986.
[25] F. Warner, *Foundations of Differentiable Manifolds and Lie Groups.* Glenview, IL: Scott, Foresman, 1971.
[26] A. Witkin, "Scale-space filtering," in *Proc. Int. Joint Conf. Artificial Intelligence*, Karlsruhe, Germany, 1983, pp. 1019–1021.

Gary A. Hewer received the B.A. degree from Yankton College, Yankton, SD, in 1962 and the M.S. and Ph.D. degrees in mathematics from Washington State University, Pullman, in 1964 and 1968, respectively.

Since 1968, he has worked at the Naval Weapons Center, China Lake, CA. Currently, he is head of the Signal Processing Technology Group. In 1986 and 1987, he was interim Scientific Officer for Applied Analysis in the Mathematics Division, Office of Naval Research. His research interests are in wavelet applications, image segmentation, total variation techniques, and the application of affine invariant partial differential equations to image processing. He is the co-holder of two patents for missile fiber optic payout design.

Dr. Heweer is a member of the Society of Photographic and Instrumentation Engineers, Sigma Xi, and the Society of Industrial and Applied Mathematics. He received the Naval Weapons Center Technical Director's Award in 1987 and the Michelson Laboratory Award in 1994.

Charles Kenney was born in Washington, DC, in 1950. He received the B.Sc., M.A., and Ph.D. degrees in mathematics from the University of Maryland, College Park, in 1973, 1976, and 1979, respectively.

From 1979 to 1981, the taught mathematics at California State College, Bakersfield, and subsequently worked as a Numerical Analyst at the Naval Weapons Center, China Lake, CA. Since 1987, he has worked half-time at the Weapons Center and half-time as a Research Engineer in the Electrical and Computer Engineering Department, University of California, Santa Barbara. His primary research is in the field of numerical linear algebra related to control theory, especially the solution of large Riccati problems via Padé approximation theory and the matrix sign function. His work in this area has led to efficient parallel algorithms with accurate condition estimation procedures. His work for the Navy has concentrated on the numerical solution of partial differential equations associated with supersonic flow over missile bodies, shock waves in detonations, thermal ablation of rocket motor linings, electromagnetic propagation in antenna horn arrays, and high-speed payout of optical fiber for missile guidance. For the last two years, his research has been in the field of image processing via PDE's.

B. S. Manjunath (M'91) received the B.E. degree in electronics (with distinction) from the Bangalore University, India, in 1985, the M.E. degree (with distinction) in systems science and automation from the Indian Institute of Science, Bangalore, in 1987, and the Ph.D. degree in electrical engineering from the University of Southern California, Los Angeles, in 1991.

He joined the Electrical and Computer Engineering Department, University of California, Santa Barbara, in 1991, where he is now an Associate Professor. During the summer of 1990, he worked at IBM T. J. Watson Research Center, Yorktown Heights, NY.

Dr. Manjunath was a recipient of the National Merit Scholarship (1978–1985) and was awarded the University Gold Medal for the best graduating student in electronics engineering in 1985 from Bangalore University. He has served on the program committees of many international conferences and workshops and was on the organizing committee of the 1997 International Conference on Image Processing. His current research interests include computer vision, learning algorithms, image/video data bases, and digital libraries. He is currently an Associate Editor of the IEEE TRANSACTIONS ON IMAGE PROCESSING.